

# Numerical simulation of cold-lap defects during casting filling process

Liu Cao<sup>1</sup> · Dunming Liao<sup>1</sup> · Fei Sun<sup>1</sup> · Tao Chen<sup>1</sup>

Received: 20 December 2017 / Accepted: 4 April 2018  
© Springer-Verlag London Ltd., part of Springer Nature 2018

## Abstract

Cold lap is one of the common defects in casting productions, which could result in poor surface accuracy and mechanical properties of castings. The cold-lap formation process is difficult to observe directly using only experimental measures, since the casting filling process is in a state of high-temperature flow inside a mold. The keys to predicting defects accurately are searching the interface front of flow, judging the collision of fronts, and defining the formation model of cold laps. A formation model of cold lap, which is related to the solid fraction, velocity, and volume fraction of the metal phase, is developed in this paper, and a method for judging the interface front and its collision was adopted. On the basis of the open-source computational fluid dynamics software OpenFOAM, a solver for predicting cold lap defects during the casting filling process was developed. The filling process of an aluminum alloy benchmark test was simulated, and the simulation results were consistent with the experimental results, which indicates the accuracy of the adopted model. Two low-pressure die-casting copper alloy filling processes with different ingates were calculated, and the formation processes of cold lap were compared with each other. The simulation results showed that there was significantly lesser cold lap in the scheme with an ingate under the lower surface of casting, which was basically consistent with the experimental results; therefore, the practicability of the adopted model was confirmed.

**Keywords** Cold lap · Formation model · Interface front · Quantitative prediction · Filling process

## Abbreviations

$t$	Time (s)	$\beta_\phi$	Solid fraction calculation factor
$U$	Velocity (m/s)	$\beta_U$	Velocity calculation factor
$C$	Surface tension coefficient (N/m)	$n$	Number of adjacent collision elements
$\kappa$	Curvature of the interface front ( $m^{-1}$ )	$U_P$	Velocity of element $P$
$\alpha$	Volume fraction	$\mathbf{n}_i$	Unit normal vector of the corresponding contact surface
$\alpha_P$	$\alpha$ value of element $P$	$\beta_g$	Cold-lap formation amount (which is a dimensionless scalar)
$\alpha_{A1}$	$\alpha$ value of one adjacent element of element $P$	$A_\beta$	Cold-lap formation constant (which is a dimensionless constant), which should be confirmed in practical production
$\alpha_{A2}$	$\alpha$ value of another adjacent element of element $P$	$\beta_b$	Accumulated amount of cold lap
$\phi$	Solid fraction of the metal phase	$\beta_c$	Current amount of cold lap
$C_{\phi 1}, C_{\phi 2}$	Two conditional expressions		
sgn	Sign function (which returns 1 when the data value is larger than 0, returns 0 when it is equal to 0, and returns -1 when it is less than 0)		
max	Larger value function (which returns the larger date value)		

## 1 Introduction

Cold lap, bifilm (entrained double oxide film), and oxide lap (asymmetric bifilm) are three of the common defects in casting productions [1]. Cold lap could result in poor surface accuracy and mechanical properties of castings, even leading to cracking and casting scraps [2]. During the casting filling process, the metal on the interface front can partially solidify

✉ Dunming Liao  
ldmhust73@163.com

<sup>1</sup> State Key Laboratory of Materials Processing and Die and Mould Technology, Huazhong University of Science and Technology (HUST), Wuhan 430074, Hubei, People's Republic of China

for various reasons, such as low pouring temperature, excessive cooling effect of the mold, and unreasonable gating system. When the partially solidified interface front collides with another interface front, cold lap can form on the collision location, causing the inadequate merging of metal, which seriously affects the casting properties [3]. The cold lap defect belongs to the well-known confluence weld defect [4], and Fig. 1 shows several images of actual castings with cold lap. Since the casting filling process is in a state of high-temperature flow inside the mold, the cold-lap formation process is difficult to observe directly using only experimental measures, which can only be applied to analyze the final cold-lap distribution of a casting [5, 6]. Possible problems during casting process can be effectively predicted by numerical simulation technology, making it possible to pre-optimize the casting process and reduce the manufacturing cost [7, 8], but there is no effective quantitative criterion for predicting cold lap at present. Therefore, searching for an accurate quantitative criterion for predicting cold lap has significance for optimizing the casting process and improving overall casting performance.

In the current research field of cold-lap prediction, the available relevant research literature is sparse, and cold-lap analysis methods are mainly indirectly a prediction of cold lap by temperature and flow simulation results, or by adopting a simple criterion [9, 10]. Vazquez et al. [11] drew the conclusion that cold lap increased distinctly with increasing tilt angle by combining simulation with experimental results. Qin et al. [12] determined the criterion that could predict the occurrence of cold lap on SUS304 stainless steel during the twin roll casting process by combining numerical simulation with test observation, and the criterion was verified by experimental results. However, the criterion is not suitable for other casting types. Hence, there is great academic and practical value in developing an accurate quantitative criterion for predicting cold lap.

Because the formation of cold lap involves the phenomena of metal liquid flow and liquid-solid conversion,

the precondition of predicting cold lap accurately is handling the effect of liquid–solid conversion on flow behavior accurately [13, 14]. Wang et al. [15] calculated the filling and solidification processes of an investment casting craft by considering that the metal would stop flowing once its solid fraction exceeded a certain threshold. Arnberg et al. [16] proposed a calculation model of viscosity realized through measurement of the solid-fraction by studying the dendrite growth process of aluminum alloys. Carman et al. [17] treated the mushy zone as porous media by studying the fluid flow through granular beds and developed a formula (the Carman-Kozeny formula) of porous media drag force with the change of solid fraction on the basis of Darcy's law [18]. After the effect of liquid–solid conversion on flow behavior is handled reasonably, quantitative prediction of cold lap means describing in detail the evolutionary process of cold lap. As a result, the keys to predicting the defect accurately are searching the interface front of flow, judging the collision of fronts, and defining the formation model of cold lap.

In this paper, the generation mechanism of cold lap during the casting filling process is explained; then, a formation model of cold lap related to the solid fraction, velocity, and volume fraction of the metal phase is developed, and a method for judging the interface front and its collision is adopted. Finally, a corresponding solver is developed on the basis of the open-source computational fluid dynamics (CFD) software OpenFOAM. For the sake of validating the accuracy and practicability of the adopted model, the filling process of an aluminum alloy benchmark test is first simulated, and the simulation results are then compared with the experimental results; afterwards, two low-pressure die-casting (LPDC) copper alloy filling processes with different ingates are calculated. The formation processes of cold lap are compared with each other, and the simulation and experimental results are also compared.

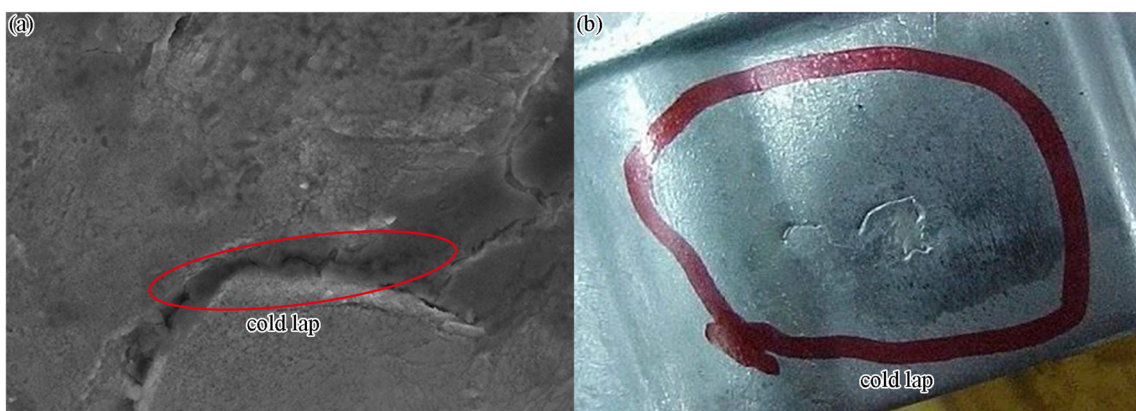


**Fig. 1** Actual castings with cold lap: **a** die casting and **b** gravity casting

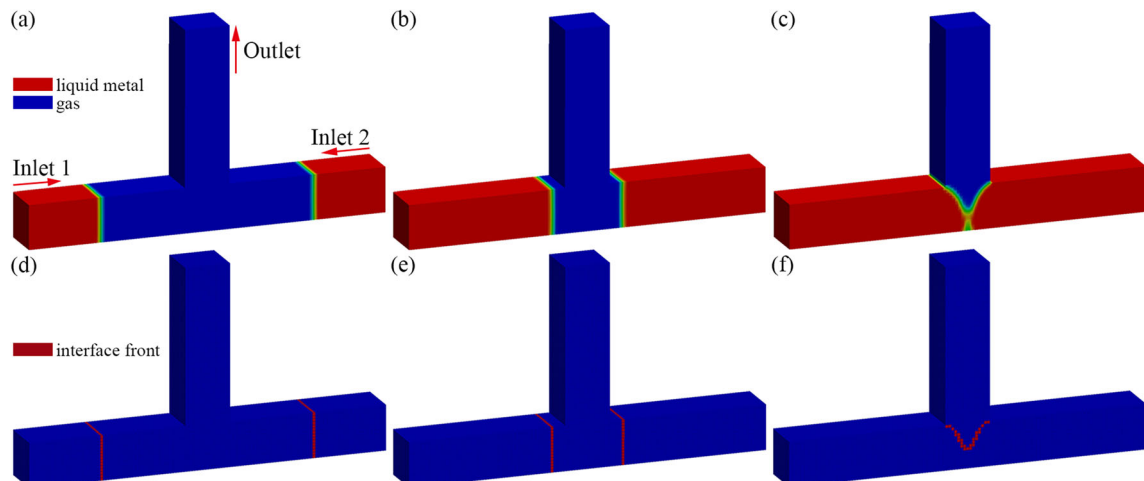


**Fig. 2** Results of interface front determination for a simple casting filling case: **a–c**  $\alpha$  distributions for different times and **d–f** corresponding determined interface fronts

## 2 Mathematical and numerical modeling

### 2.1 Determination of interface front and its collision

The precondition of determining the interface front of flow is the corresponding algorithm for representing the interface front, which falls into two major categories: interface tracking [19] and interface capturing [20]. In interface tracking methods, the interface front is tracked explicitly by mesh or particles, but the geometric topology change cannot be handled well for the complex interface front; in interface capturing methods, the interface front is represented by the volume fraction of each element, so it is fit for handling the complex geometric topology change and considering the effect of surface tension. The volume of fluid (VOF) [21] algorithm is the most widely known interface capturing method. Considering that the interface front changes sharply during the casting filling process, the VOF algorithm is adopted here to track

the interface front. The volume fraction  $\alpha$  that represents the volume fraction of the metal phase at different locations is used in the VOF algorithm. The value 1 of  $\alpha$  means that the metal phase completely occupies the location, and the value 0 means the contrary situation, so the value of  $\alpha$  around the interface is between 0 and 1. The volume-fraction equation [20] that controls the distribution rule of  $\alpha$  is

$$\frac{\partial \alpha}{\partial t} + \nabla \cdot (\alpha \mathbf{U}) = 0 \quad (1)$$

In this paper, the continuum surface force (CSF) [22] model is adopted to treat the surface tension of two-phase flow, which can be used to obtain the continuous pressure distribution; thereby, the surface tension  $\mathbf{F}_s$  at the interface front can be obtained by

$$\mathbf{F}_s = C\kappa \nabla \alpha \quad (2)$$

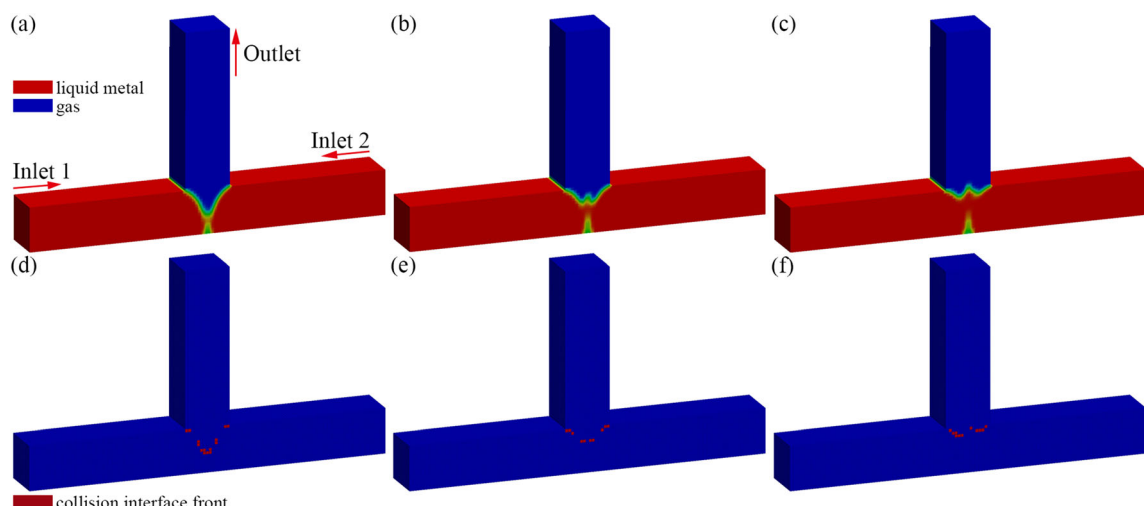


**Fig. 3** Collision elements for a simple casting filling case: **a–c**  $\alpha$  distributions for different times and **d–f** corresponding determined collision elements

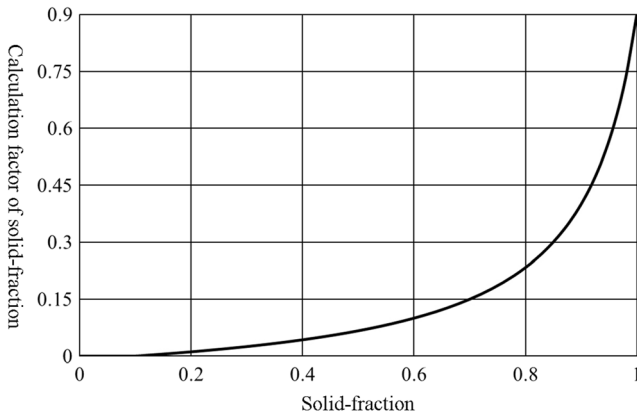


**Fig. 4** Changing curve of  $\beta_\phi$

When the interface front of flow is obtained by  $\alpha$ , a very rough interface front will be obtained, if all the elements with  $\alpha$  values between 0 and 1 are regarded on the interface front. The reason for obtaining a rough interface front is the unavoidable interfacial diffusion phenomenon in interface capturing methods, which means that the  $\alpha$  values of multiple adjacent elements are between 0 and 1. Considering that the interface front needed here should be the possible location of cold lap, the strategy for determining the interface front is proposed below. First, the  $\alpha$  value of each element is extracted, which should be between 0.1 and 0.9; second,  $\alpha$  values of the adjacent elements are extracted, and the  $\alpha$  value of one adjacent element should be above 0.7 and another should be below 0.3. The interface front elements are the elements that simultaneously satisfy the two conditions above, and the formula for determining the interface front is

$$\left\{ \begin{array}{l} 0.1 < \alpha_P < 0.9 \\ \alpha_{A1} > 0.7 \& \& \alpha_{A2} < 0.3 \end{array} \right. \quad (3)$$

Figure 2 shows the results of the interface front determined by adopting Eq. (3), for a simple casting filling case. From the results, the searched results of the interface front (Fig. 2d–f) coincide well with the  $\alpha$  distributions (Fig. 2a–c), which certifies the validity of the developed method for determining the interface front.

Owing to the fact that cold lap is generated at the intersection of interface fronts, the collision of interface fronts should be determined after the interface front has been found, which means that the interface front elements about to collide in the next time step should be determined. The strategy for determining the collision of interface fronts is proposed below. First, the element itself and at least one adjacent element are both interface front elements; second, the velocities of the element itself and the adjacent element should both be across the contact surface. To be specific, when the element itself and one adjacent element are both interface front elements, the two elements can be thought to collide immediately, under one of the three situations: (1) the velocity of the element itself is zero or parallel to the contact surface, and the velocity of the adjacent element is parallel to the contact surface; (2) the velocity of the element itself is parallel to the contact surface, and the velocity of the adjacent element is zero or parallel to the contact surface; and (3) the velocities of the element itself and the adjacent element are both parallel to the contact surface. Figure 3 shows the collision elements determined using the method described above, for a simple casting filling case. From the determined results, the searched results of collision elements (Fig. 3d–f) coincide well with the  $\alpha$  distributions (Fig. 3a–c), which certifies the validity of the method developed for determining interface front collision.

## 2.2 Formation model of cold lap

After obtaining the interface front and its collision, the key to predicting cold lap is calculating its formation. Considering that the intensity of cold-lap generation mainly depends on the solidification and collision status of the interface front, cold-lap formation is calculated on the basis of three factors: solid fraction  $\phi$ , velocity  $\mathbf{U}$ , and volume fraction  $\alpha$  of the metal phase.

### (1) Solid fraction calculation factor

Cold lap may be generated only when the interface front has been partially solidified. We consider that  $\phi$  has an effect on the formation of cold lap when it is higher than 0.1, so a conditional expression can be written as follows:

$$C_{\phi 1} = \text{sgn}(\max(\phi - 0.1, 0.0)) \quad (4)$$

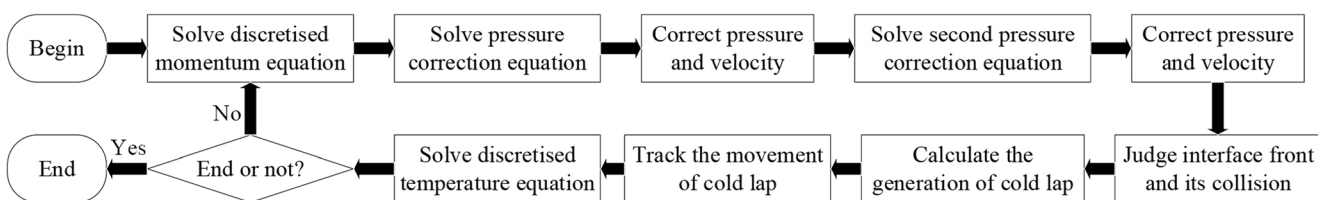
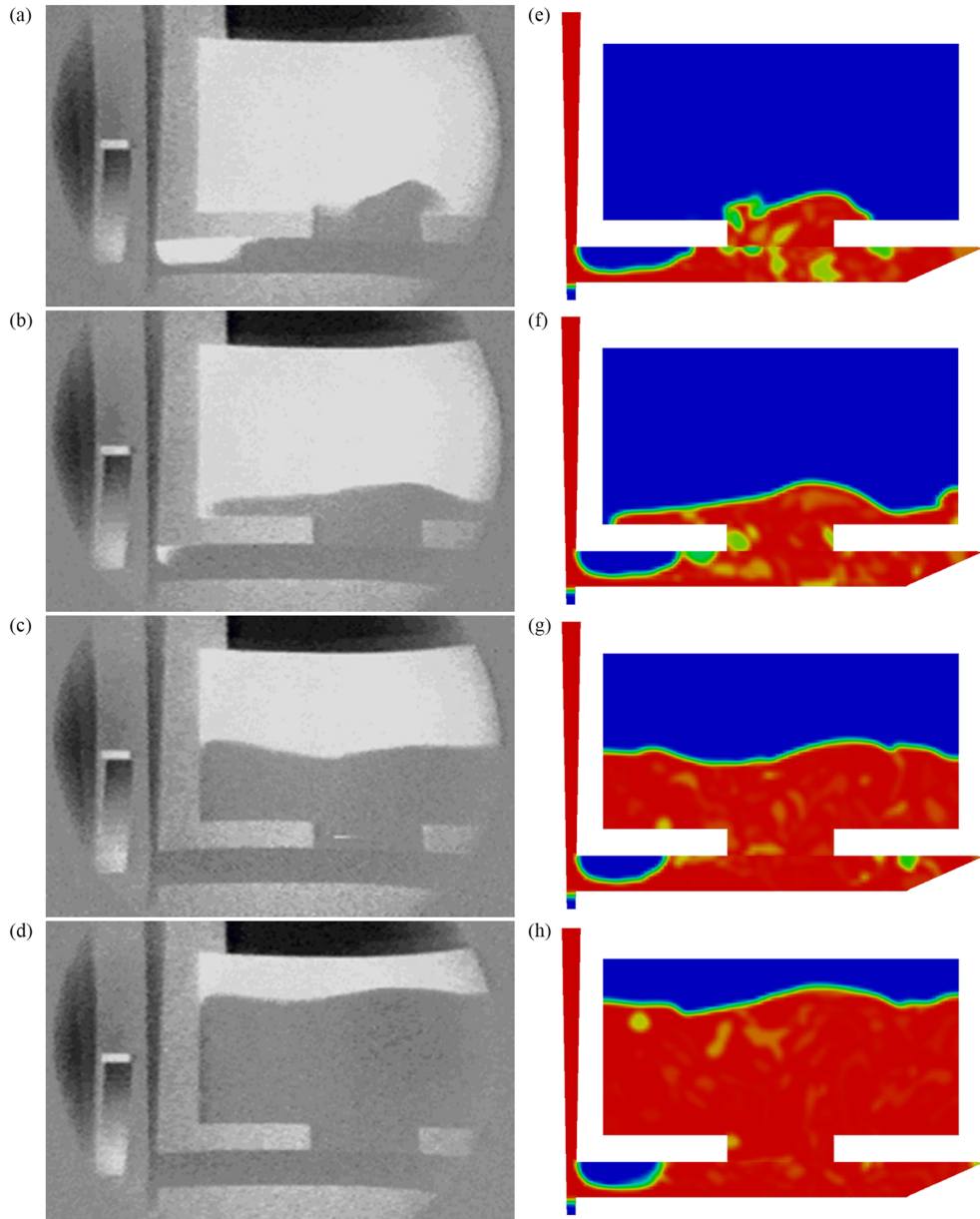


**Fig. 5** General calculation process

**Fig. 6** Interface shape of the benchmark test in the experimental results (left) and simulation results (right) at different times: **a, e** 1.55 s, **b, f** 1.75 s, **c, g** 2.45 s, and **d, h** 3.20 s



In consideration of the fact that the nearer the collision interface front approximates the solid phase, the more obvious cold lap will be. The calculation factor is proposed as follows:

$$C_{\phi 2} = \frac{0.1}{1.1-\phi} - 0.1 \quad (5)$$

By combining Eqs. (4) and (5), the solid fraction calculation factor  $\beta_\phi$  can be obtained by

$$\beta_\phi = C_{\phi 1} \cdot C_{\phi 2} = \left( \frac{0.1}{1.1-\phi} - 0.1 \right) \cdot \text{sgn}(\max(\phi - 0.1, 0.0)) \quad (6)$$

**Table 1** Parameters used for the simulation

Parameter	Value	Unit
Aluminum density	2385	kg/m <sup>3</sup>
Air density	1	kg/m <sup>3</sup>
Aluminum dynamic viscosity	$3.1 \times 10^{-3}$	Pa·s
Air dynamic viscosity	$1 \times 10^{-5}$	Pa·s
Aluminum-air surface tension coefficient	0.871	N/m
Acceleration of gravity	{0, -9.8, 0}	m/s <sup>2</sup>
Inlet velocity	{0, -0.31, 0}	m
Pouring temperature	720	°C

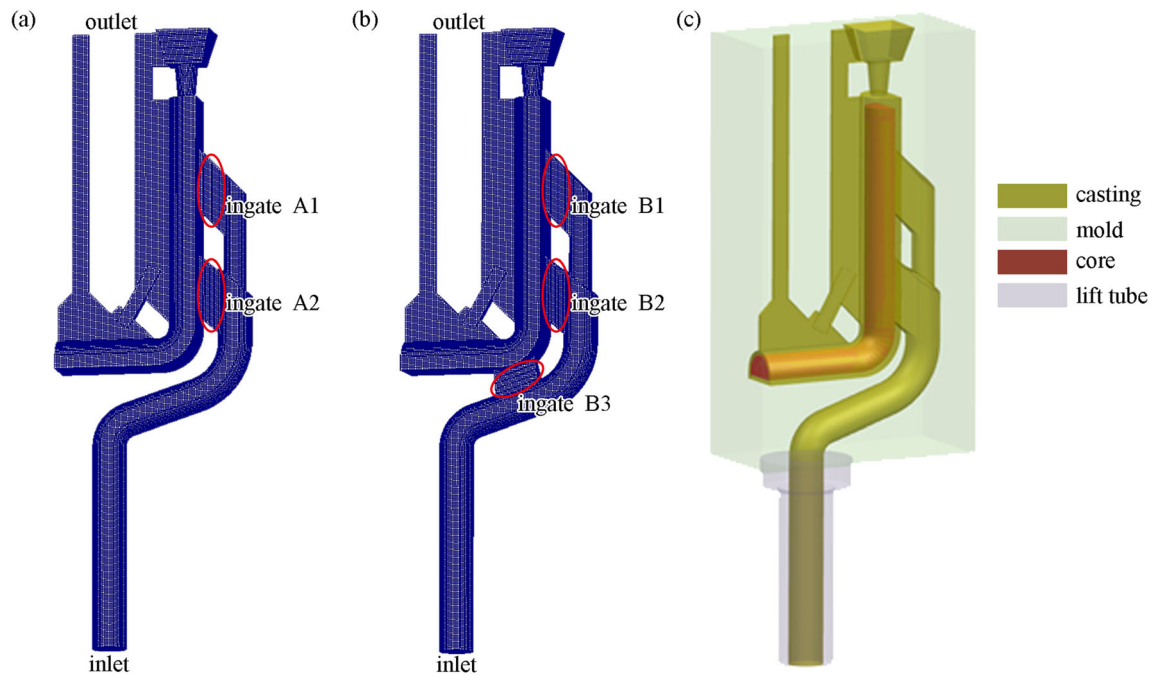


**Fig. 7** Geometric model and mesh of the adopted LPDC schemes: **a** Scheme 1, **b** Scheme 2, and **c** parts of Scheme 1

Figure 4 shows the change curve of  $\beta_\phi$ . As can be seen from the figure, when  $\phi$  is less than 0.1,  $\beta_\phi$  is 0, which means no cold lap occurs. When  $\phi$  is at a low level,  $\beta_\phi$  slowly increases with increasing  $\phi$ , which means little formation of cold lap under low  $\phi$ . When  $\phi$  is at a high level,  $\beta_\phi$  rapidly increases with increasing  $\phi$  (the value of  $\beta_\phi$  under  $\phi = 1$  is 13.5 times higher than under  $\phi = 0.5$ ), which means a large formation of cold lap under high  $\phi$ .

## (2) Velocity calculation factor

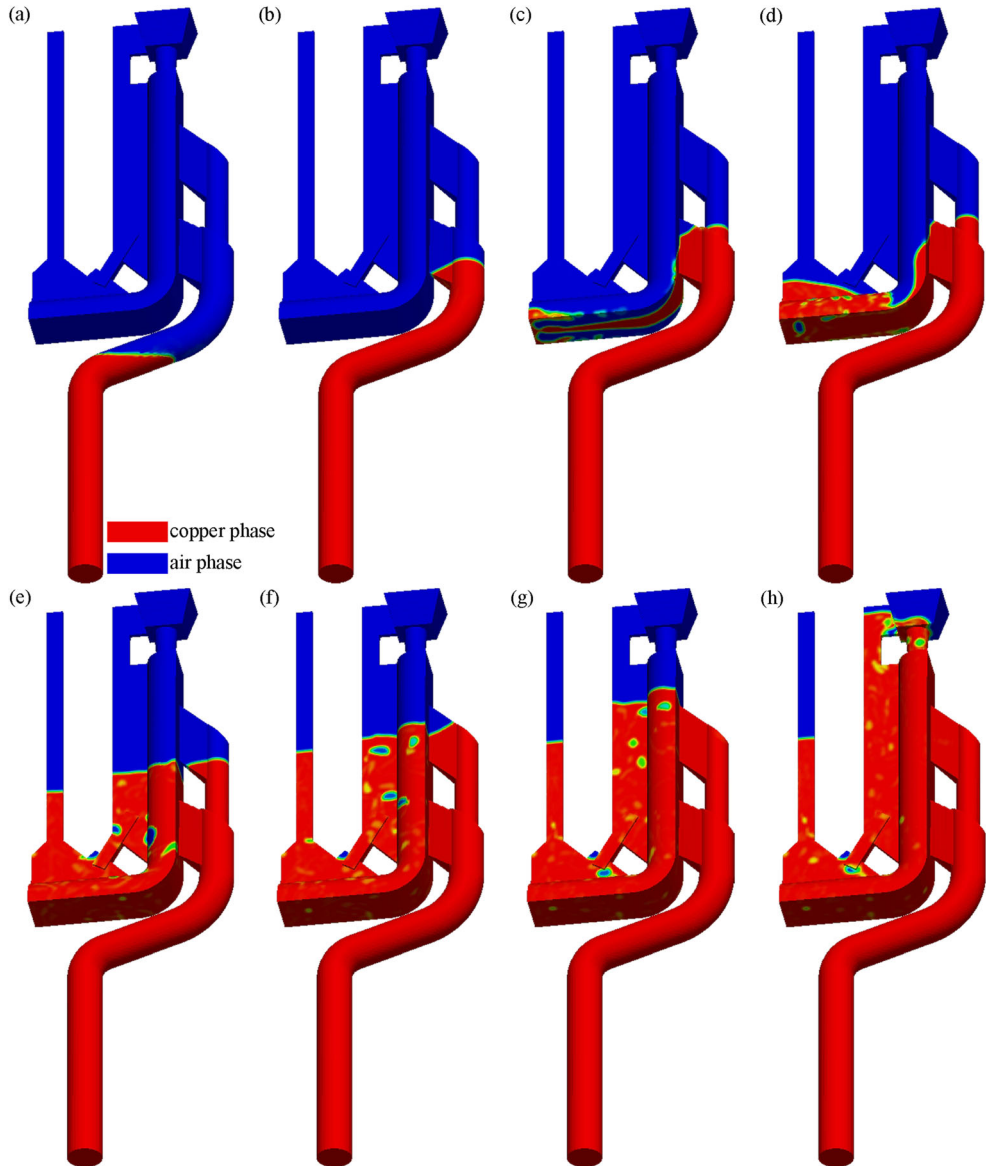
$U$  can be used to represent the intensity of the interface front collision; specifically, the normal component of the element velocity on the contact surface denotes the intensity of collision. In consideration of more than one adjacent collision element, the corresponding contact surfaces must be calculated one by one; therefore, the velocity calculation factor  $\beta_U$  is expressed as follows:

$$\beta_U = \sum_{i=1}^n \mathbf{U}_P \cdot \mathbf{n}_i \quad (7)$$

**Table 2** Parameters used for the calculation

Parameter	Value	Unit
Copper alloy density	7000	kg/m <sup>3</sup>
Air density	1	kg/m <sup>3</sup>
Copper alloy dynamic viscosity	$3.22 \times 10^{-3}$	Pa·s
Air dynamic viscosity	$1 \times 10^{-5}$	Pa·s
Copper alloy-air surface tension coefficient	1.2	N/m
Copper alloy specific heat	480	J/kg/K
Copper alloy heat conductivity	120	W/m/K
Copper alloy liquidus temperature	921.4	°C
Copper alloy solidus temperature	890	°C
Copper alloy latent heat	$1.53 \times 10^5$	J/kg
Acceleration of gravity	{0, 0, -9.8}	m/s <sup>2</sup>
Inlet pressure	0(0 s); 0.38(5 s); 0.38(10 s)	bar
Pouring temperature	1010	°C
Constant of cold lap formation	1	none
Casting-lift tube interfacial heat-transfer coefficient	500	W/m <sup>2</sup> /K
Casting-mold interfacial heat-transfer coefficient	1500	W/m <sup>2</sup> /K
Casting-core interfacial heat-transfer coefficient	500	W/m <sup>2</sup> /K

**Fig. 8** Copper phase distributions at different times in Scheme 1: **a** 1.45 s, **b** 2.30 s, **c** 2.70 s, **d** 3.10 s, **e** 3.75 s, **f** 4.10 s, **g** 4.30 s, and **h** 4.70 s



### (3) Calculation factor of metal phase volume

$\alpha$  denotes the metal phase volume in the collision element, and cold lap here is supposed to be linearly related to the metal phase volume. Hence, the calculation factor  $\beta_\alpha$  of the phase volume is expressed as follows:

$$\beta_\alpha = \alpha \quad (8)$$

Integrating the calculation factors above [Eqs. (6)–(8)], the formation model of cold lap can be formulated as

$$\beta_g = A_\beta \beta_\phi \beta_U \beta_\alpha = A_\beta \cdot \left( \frac{0.1}{1.1 - \phi} - 0.0909 \right) \cdot \text{sgn}(\max(\phi - 0.1, 0)) \cdot \left( \sum_{i=1}^n \mathbf{U}_p \cdot \mathbf{n}_i \right) \cdot \alpha \quad (9)$$

### 2.3 Tracking cold-lap movement and calculation methodology

After accessing the cold-lap formation model, the movement of cold lap during the casting filling process is tracked by the transport equation, as follows:

$$\frac{\partial \beta_b}{\partial t} + \nabla \cdot (\mathbf{U} \beta_b) = 0 \quad (10)$$

The current amount of cold lap  $\beta_c$  can then be determined by the following:

$$\beta_c = \beta_b + \beta_g \quad (11)$$

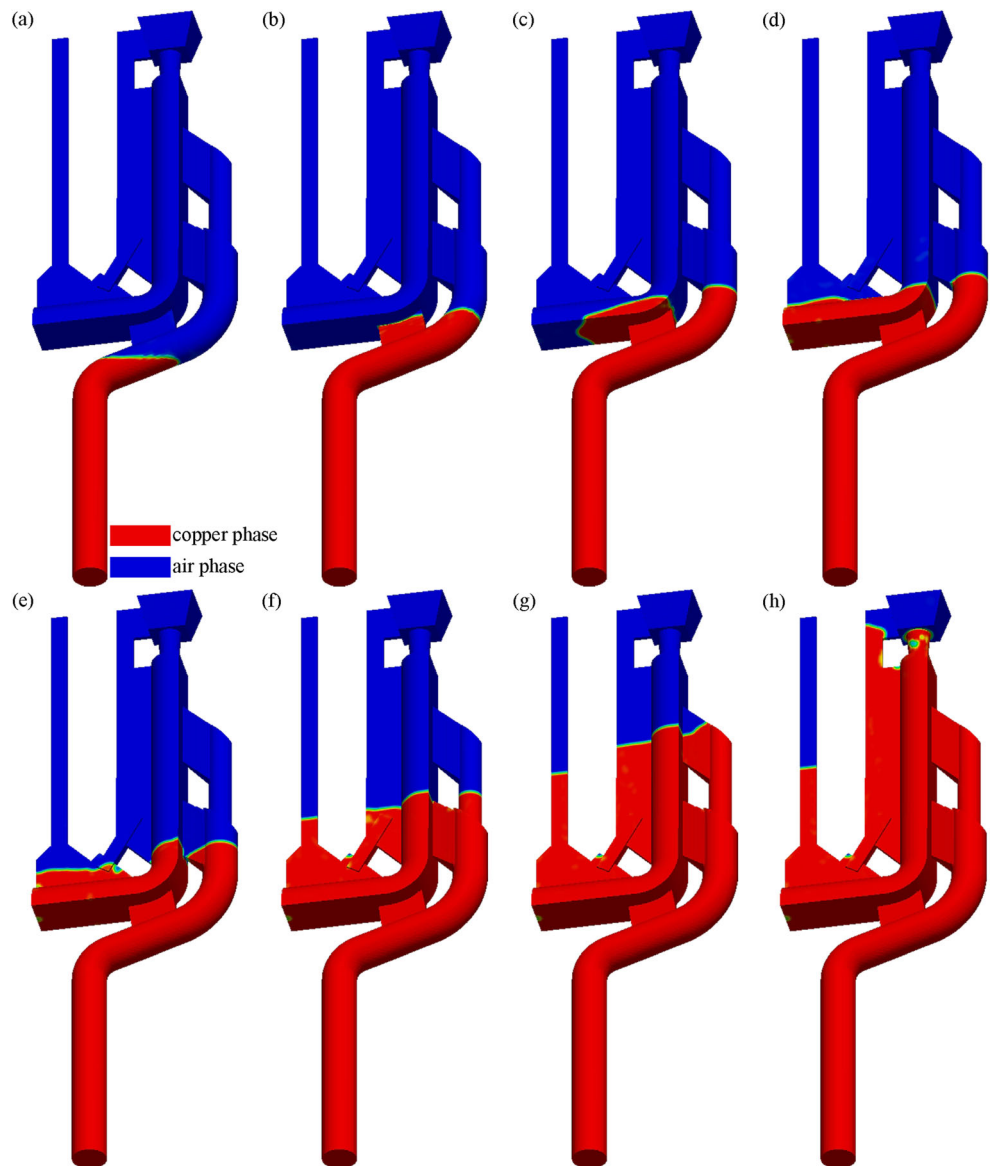
Implementation of the calculation code in this paper was based on the solver InterFoam [23] in OpenFOAM software; OpenFOAM is one of the most widely used open-source CFD software packages. Some functions were appended on the base of the solver InterFoam, including solving temperature field, determining interface front and its collision, calculating cold-lap generation, tracking cold-lap movement, etc. In this paper, the PIMPLE algorithm [24] was introduced into the coupled solution of the pressure and velocity. The PIMPLE algorithm is the combination of SIMPLE (Semi-Implicit Method for Pressure-Linked Equations) [25] algorithm and PISO (Pressure Implicit with Splitting of Operators) [26], which means that the SIMPLE algorithm is used for the steady computing in each time step, and the stepping of time step is realized by the PISO algorithm. It should be noted that details of the solidification model (such as the latent heat release, the

momentum source term in the mushy zone, etc) can be found in Ref. [27]. The general calculation process in this paper is shown in Fig. 5.

### 3 Results and discussion

Based on the mathematical and numerical model presented above, the calculation code for predicting cold lap during the casting filling process was developed on the foundation of the InterFoam solver. In order to verify the accuracy and practicability of the adopted model, the filling process of an aluminum alloy benchmark test [28] was first calculated, and the simulation results were then compared with the experimental results. Second, two LPDC copper alloy filling processes with different ingates were simulated, and the cold-lap formation

**Fig. 9** Copper phase distributions at different times in Scheme 2: **a** 1.45 s, **b** 2.05 s, **c** 2.35 s, **d** 2.70 s, **e** 2.95 s, **f** 3.60 s, **g** 4.20 s, and **h** 4.75 s



processes were compared with each other, and simulation results were compared with experimental results. In addition, the mesh-generation tool used here was ICEM CFD [29], and the open-source software ParaView [30] was used for post-processing.

### 3.1 Aluminum alloy benchmark test

The aluminum alloy benchmark test of the filling process was designed by Campbell [28], and the casting in it was a plate measuring 200 mm × 100 mm × 10 mm. An unclosed bottom gating system was adopted in the benchmark test. The mold cavity was made of resin-bonded sand, and its shape and size, as well as the experimental gating system, are shown in Ref. [31]. During the filling process, the interface shape of the liquid metal was recorded with in situ X-ray imaging technology. The pouring liquid was 99.999% pure aluminum, and the parameters used for the simulation are listed in Table 1.

Figure 6 shows the interface shape of the liquid metal in the experimental and simulation results at different times. From the comparison results, at time 1.55 s (Fig. 6a, e), the interface front of the liquid flowed to the ingate, and the right of it was obviously higher; meanwhile, a large, closed air mass was formed to the left of the cross-gate, and the simulation results are in good agreement with experiment. At time 1.75 s (Fig. 6b, f), the liquid was spread on the bottom surface of the plate, and a crest was formed on the middle-right of the interface front. The large closed air mass still existed in the left of the cross-gate in the simulation, but there was only a small amount of air in the experiment. The reason may be that the

sand mold was thought to be airtight in the calculation, and air could be expelled along the coarse surface of sand mold in the experiment. At times 2.45 s (Fig. 6c, g) and 3.20 s (Fig. 6d, h), the filling heights of the simulation and experimental results were basically the same. Generally speaking, the simulation results are basically consistent with the experimental results, which verifies the accuracy of the mathematical and numerical models in this paper.

### 3.2 Calculation and experimental analysis of cold lap in copper alloy LPDC processes

To further prove the practicability of the adopted model, two LPDC copper alloy filling processes (Schemes 1 and 2) with different ingates were simulated, the cold-lap formation processes were compared with each other, and the simulation results were compared with the experimental results. Figure 7 shows the geometric model and mesh of the two schemes; the only difference between them is the ingate B3 (Fig. 7b) on the bottom of the casting in Scheme 2. The overall dimensions of the casting are 174 mm × 41 mm × 552 mm, and the casting is of curved-tube construction, the thickness of which is 4 mm. The copper alloy material used in the experiment was GKMS60. Table 2 lists the parameters used for the calculation, and the contact relations between different parts can be obtained from Fig. 7c.

Figure 8 illustrates the copper phase distributions at different times during the casting filling process in Scheme 1. From the simulation results, the liquid metal could first flow into the cavity only through ingate A2 (Fig. 8a, b); the liquid ran to the

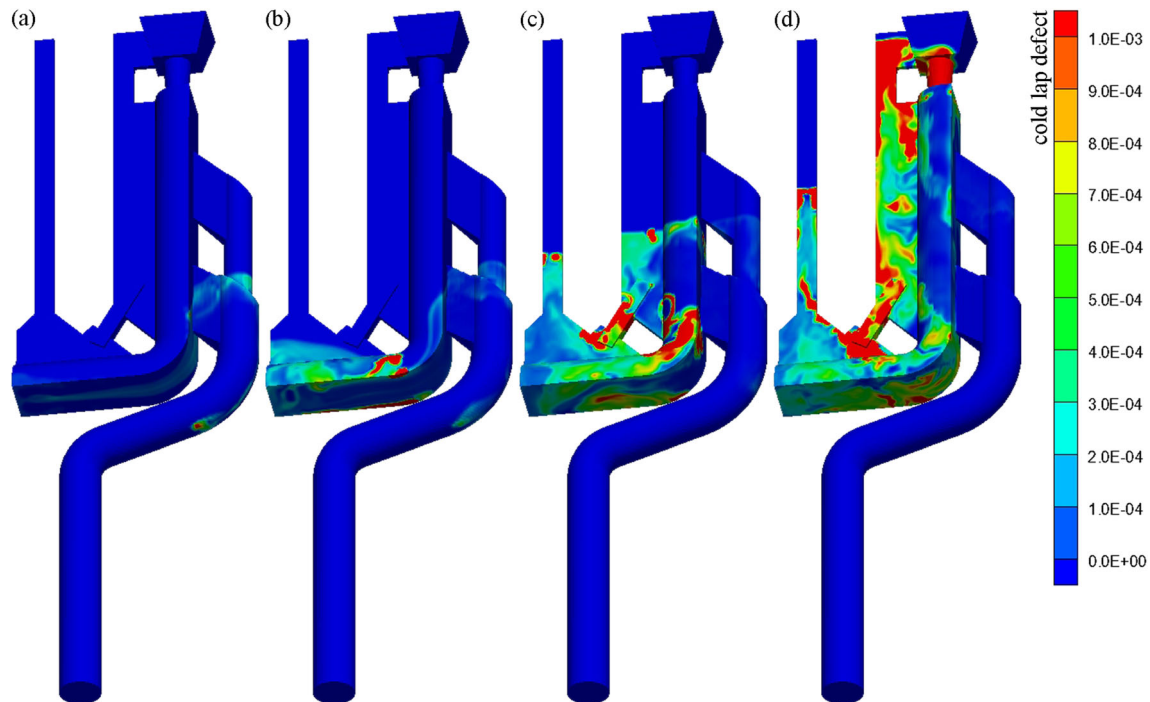


**Fig. 10** Cold-lap distributions at different times in Scheme 1: **a** 2.70 s, **b** 3.10 s, **c** 3.75 s, and **d** 4.70 s

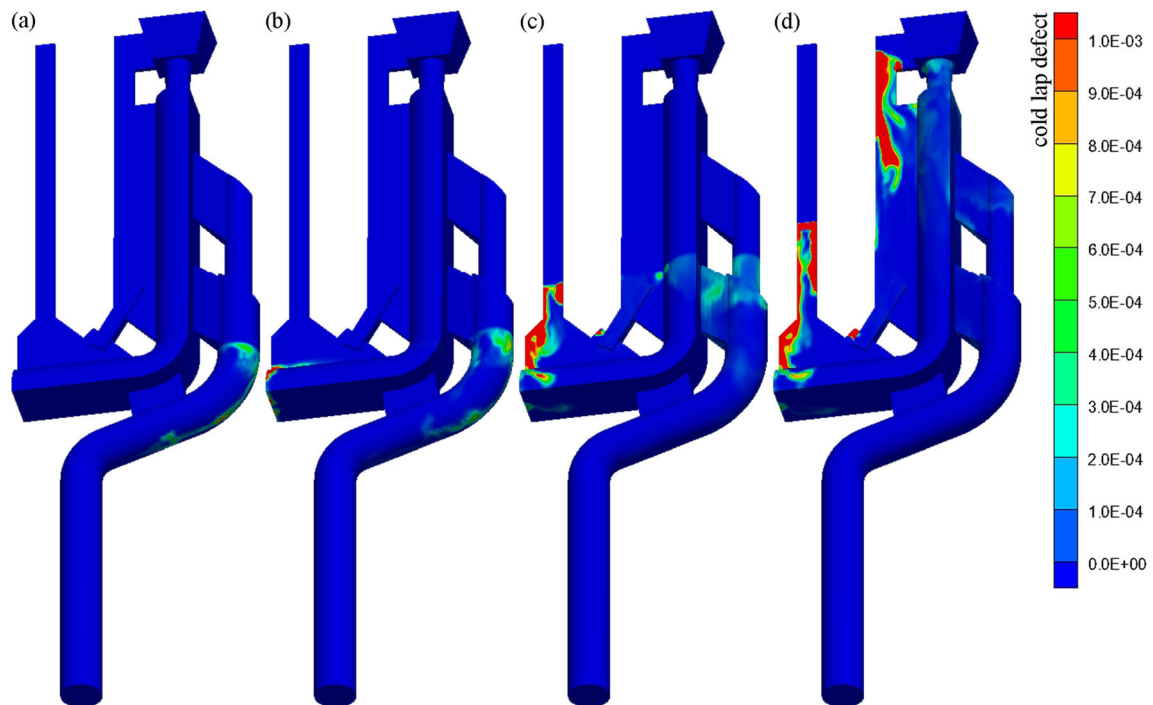


**Fig. 11** Cold-lap distributions at different times in Scheme 2: **a** 2.35 s, **b** 2.70 s, **c** 3.60 s, and **d** 4.75 s

bottom of the casting from ingate A2, owing to the location of ingate A2 being higher than that of the bottom, which led to the disorganized flow on the bottom from the effect of gravity (Fig. 8c, d). When the liquid flowed to ingate A1, the liquid could flow into the cavity through both ingates A1 and A2, and the casting filling process was smooth (Fig. 8e–h). Figure 9 illustrates the copper phase distributions at different times during the casting filling process in Scheme 2. From the simulation results, the liquid metal first flowed into the cavity through ingate B3, and the flow was steady on the bottom of casting, owing to the location of ingate B3 being lower than that of the bottom (Fig. 9a–d); the flow was also steady when the liquid flowed to ingates B2 and B1 (Fig. 9e–h).

Figures 10 and 11 show the cold-lap distributions at different times during the casting filling process in

Schemes 1 and 2, respectively. From the simulation results shown in Fig. 10, significant cold lap was generated on the lower part of the casting, because the flow was disorganized on the bottom and the liquid metal had cooled quickly (Fig. 10a–c). A small amount of cold lap appeared on the upper part of the casting, because of the smooth flow in it and because of the heat-preservation effect of ingate A1 (Fig. 10d). From the simulation results shown in Fig. 11, the casting exhibited hardly any cold lap on account of the smooth flow during the entire filling process. Moreover, it should be noted that some cold lap was generated on the upper left of the casting in both Schemes 1 and 2, because the upper left of the casting is a thin exhaust plate and the metal cooled quickly on the plate. Therefore, the cold lap that formed here should not be considered, since it has little

**Fig. 12** Comparison of the simulation results of cold lap on the casting bottom in the two schemes: **a** chosen curve and **b** comparison of cold-lap simulation results

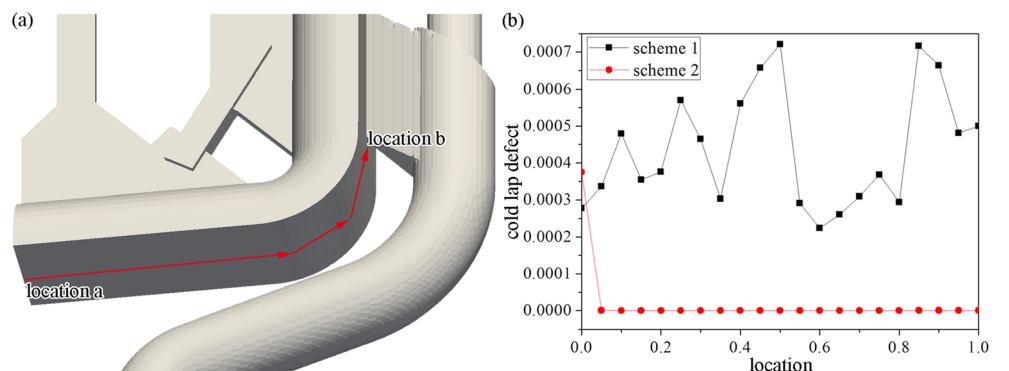
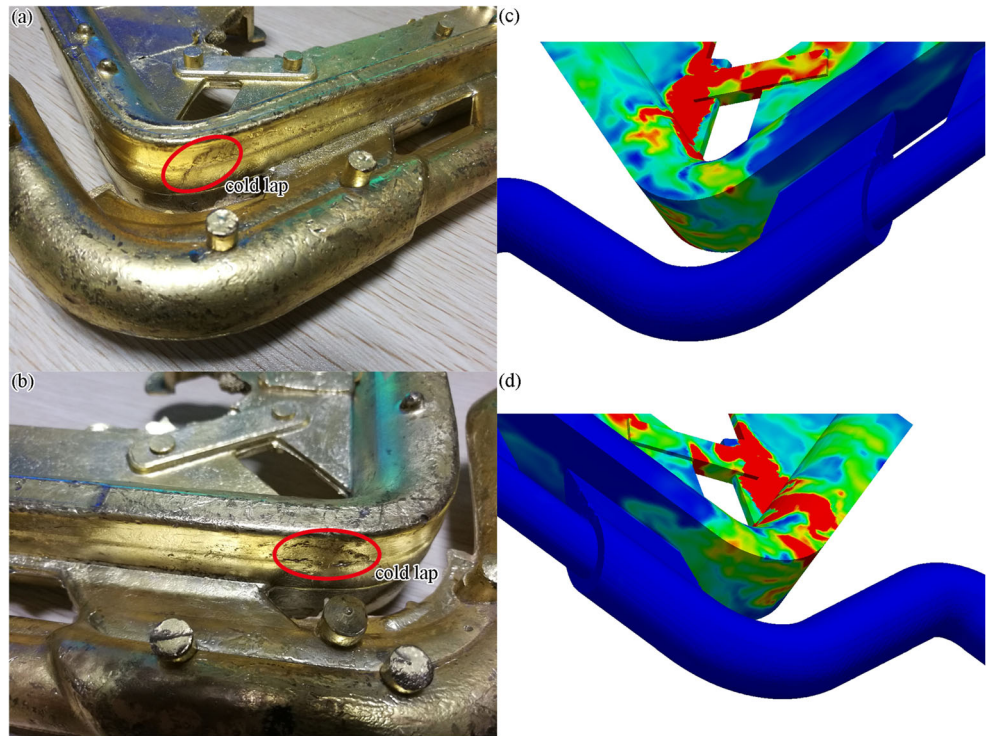


**Fig. 13** Comparison between actual cold lap with the simulation results in Scheme 1: **a, b** actual cold lap and **c, d** simulation cold-lap results



influence on the casting. In order to compare the cold-lap distributions in the two schemes quantitatively, a curve shown in Fig. 12a was chosen, in consideration that the cold lap on the bottom in the two schemes differed most significantly. The values along the curve (from location a to location b) were extracted in the two schemes and compared in Fig. 12b. From the comparison results, it is evident that the amount of cold lap in Scheme 1 is much greater than that in Scheme 2, and there is only a small amount of cold lap on the left of the bottom in Scheme 2.

Figure 13 shows the comparison of the actual cold lap with the simulation results in Scheme 1. From the comparison results, there is apparent cold lap on the corner of the actual casting (Fig. 13a, b), the reason being that the liquid metal cooled quickly in the process of flowing on the bottom. The partially solidified interface front below then collided with the one above when the front rose to the corner, which formed cold lap owing to the inadequate merging of metal. From the cold-lap simulation results (Fig. 13c, d), there was also apparent cold lap on the corner of the casting. The cold-lap locations in the experimental and simulation results do not precisely correspond with each other, because cold-lap formation is related to the dendrite growth; however, the cold-lap prediction model presented here does not consider dendrite growth at the micro level. Dendrite growth cannot be considered in the current macro simulation, and the actual cold lap is basically on the area with a larger defect prediction value. Therefore, the practicability of the adopted model is verified.

## 4 Conclusions

- (1) To predict cold-lap defects during the casting filling process, a cold-lap formation model related to solid fraction, velocity, and volume fraction of the metal phase, was developed, and a method for determining the interface front and its collision was adopted. Using the open-source CFD software OpenFOAM, a solver for predicting cold lap during the casting filling process was developed.
- (2) The parameter (constant of cold-lap formation  $A_\beta$ ) in the quantitative cold-lap model should be confirmed in practical production.
- (3) The filling process of an aluminum alloy benchmark test was simulated, and the simulation results were consistent with the experimental results, which verifies the accuracy of the adopted model.
- (4) Two low-pressure die-casting copper alloy filling processes with different ingates were calculated, and the cold-lap formation processes were compared with each other. The simulation results show that there was significantly lesser cold lap in the scheme with an ingate under the lower surface of the casting, which was basically consistent with experimental results; therefore, the practicability of the adopted model was confirmed.

**Acknowledgments** This research is supported by the Program for New Century Excellent Talents in University (NCET-13-0229) and the National Science and Technology Key Projects of Numerical Control (2012ZX04010-031).

We would like to thank LetPub ([www.letpub.com](http://www.letpub.com)) for providing linguistic assistance during the preparation of this manuscript.

## Compliance with ethical standards

**Conflict of interest** The authors declare that they have no conflict of interest.

**Publisher's note** Springer Nature remains neutral with regard to jurisdictional claims in published maps and institutional affiliations.

## References

- Campbell J (2011) Complete casting, handbook, metal casting process, metallurgy, techniques and design. Butterworth-Heinemann, United Kingdom
- Rajkolhe R, Khan JG (2014) Defects, causes and their remedies in casting process: a review. *Int J Res Advent Technol* 2(3):375–383
- JadHAV B, JadHAV SJ (2013) Investigation and analysis of cold shut casting defect and defect reduction by using 7 quality control tools. *Int J Adv Eng Res Stud* 2(4):28–30
- Hsu FY, Yang YM (2012) Confluence weld in an aluminum gravity casting. *J Mater Process Technol* 212(4):825–840
- Li CY, Wu SP, Guo JJ, Su YQ, Bi WS, Fu HZ (2006) Model experiment of mold filling process in vertical centrifugal casting. *J Mater Process Technol* 176(1):268–272
- Zhang W, Xie G, Zhang D (2010) Application of an optimization method and experiment in inverse determination of interfacial heat transfer coefficients in the blade casting process. *Exp Thermal Fluid Sci* 34(8):1068–1076
- Dabade UA, Bhedasgaonkar RC (2013) Casting defect analysis using design of experiments (DoE) and computer aided casting simulation technique. *Procedia CIRP* 7:616–621
- Liu DR, Yang ZP, Wang LP, Guo EJ (2016) Development of simulation of mould filling during casting: a review. *J Harbin Univ Sci Technol* 21(3):96–100
- Xiao L, Anzai K, Niyama E, Kimura T, Kubo H (1998) Reducing “cold shut” defects in the “H” process aided by computer simulation. *Int J Cast Metal Res* 11(2):71–81
- Lee JH, Won CW, Cho SS, Chun BS, Kim SW (2000) Effects of melt flow and temperature on the macro and microstructure of scroll compressor in direct squeeze casting. *Mater Sci Eng A* 281(1):8–16
- Vazquez V, Juarez-Hernandez A, Mascarenas A, Zambrano P, Hernandez-Rodriguez MAL (2010) Cold shut formation analysis on a free lead yellow brass tap. *Eng Fail Anal* 17(6):1285–1289
- Qin YJ, Sun GX, Yu WP, Ni SK (1997) Criterion for predicting cold shut mark. *Shanghai Metal* 19(5):23–27
- Lewis RW, Ravindran K (2000) Finite element simulation of metal casting. *Int J Numer Meth Eng* 47(1–3):29–59
- Frehse J, Málek J, Steinhauer M (2003) On analysis of steady flows of fluids with shear-dependent viscosity based on the Lipschitz truncation method. *SIAM J Math Anal* 34(5):1064–1083
- Wang C, Hu H, Luo J (2007) Computer simulation of investment casting based on Procast software. *Foundry Technol* 28(10):1360–1365
- Amberg L, Bäckerud L, Chai G (1996) Solidification characteristics of aluminum alloys: dendrite coherency. American Foundrymen's Society, Schaumburg
- Carman PC (1937) Fluid flow through granular beds. *T-I. Chem Eng* 15:150–166
- Whitaker S (1986) Flow in porous media I: a theoretical derivation of Darcy's law. *Transport Porous Med* 1(1):3–25
- Bridson R, Hourihane J, Nordenstam M (2007) Curl-noise for procedural fluid flow. *ACM T Graph (TOG)* 26(3):46
- Hirt CW, Nichols BD (1981) Volume of fluid (VOF) method for the dynamics of free boundaries. *J Comput Phys* 39(1):201–225
- Ménard T, Tanguy S, Berlemon A (2007) Coupling level set/VOF/ghost fluid methods: validation and application to 3D simulation of the primary break-up of a liquid jet. *Int J Multiphas Flow* 33(5):510–524
- Brackbill JU, Kothe DB, Zemach C (1992) A continuum method for modeling surface tension. *J Comput Phys* 100(2):335–354
- OpenFOAM Foundation Ltd (2016) OpenFOAM User Guide V4.0
- Tobias Holzmann. Mathematics (2017) Numerics, Derivations and OpenFOAM(R). Holzmann CFD, Leoben
- Patankar SV, Spalding DB (1972) A calculation procedure for heat, mass and momentum transfer in three-dimensional parabolic flows. *Int J Heat Mass Transf* 15(10):1787–1806
- Issa RI, Gosman AD, Watkins AP (1986) The computation of compressible and incompressible recirculating flows by a non-iterative implicit scheme. *J Comput Phys* 62(1):66–82
- Cao L, Sun F, Chen T, Teng ZH, Tang YL, Liao DM (2017) Numerical simulation of liquid-solid conversion affecting flow behavior during casting filling process. *Acta Metall Sin*. <https://doi.org/10.11900/0412.1961.2017.00083>
- Sirrell B, Holliday M, Campbell J (1995) The benchmark test 1995. 7th conference on modeling of casting welding and solidification, London
- Lei X, Huixin L (2008) The technology of numerical simulation based on ANSYS ICEM CFD and CFX software. *Mech Eng* 12:65–66
- Henderson A, Ahrens J, Law C (2004) The ParaView Guide
- Pang SY, Chen LL, Zhang MY, Yin YJ, Chen T, Zhou JX, Liao DM (2010) Numerical simulation two phase flows of casting filling process using SOLA particle level set method. *Appl Math Model* 34(12):4106–4122